Investigation on Wave Behaviour at Defects in 2D Composite Structures Using Spectral Finite Elements in the Time Domain

B. HENNINGS and R. LAMMERING

ABSTRACT

The understanding of the propagation behaviour of high frequency elastic waves (Lamb waves) in thin-walled layered structures is a very important basis of structural health monitoring (SHM) in large-scale constructions.

This paper deals with the numerical simulation of the wave propagation using the spectral finite element method (SFEM) in the time domain. In the following, this method is explained and investigations in a 7-ply composite consisting of unidirectional layers and twill weaves are presented. In this context, the employed delamination model obtained by node separation is compared with a delamination model made up of contact elements.

INTRODUCTION

The complete inspection of lightweight structures for defects, e.g. by scanning inspection methods, is cost-intensive and time-consuming. Therefore, structural health monitoring methods which use the selective excitation and propagation of high-frequency elastic waves (Lamb waves) are currently under investigation, especially for possible use in carbon fibre reinforced plastics (CFRP), e.g. for detection, localisation and assessment of delaminations. In order to further develop this technology and to better understand the related phenomena, computational analysis of Lamb waves has become a very important issue.

Since analytical computation of lightweight shell and plate structures is limited to

Bianca Hennings, Rolf Lammering
Helmut-Schmidt-Universität, Universität der Bundeswehr Hamburg
Fakultät für Maschinenbau, Institut für Mechanik
Holstenhofweg 85, D-22043 Hamburg
bianca.hennings@hsu-hh.de

simple boundary and loading conditions, numerical methods, such as finite element method (FEM), boundary element method (BEM) or the spectral element method in the frequency domain, have been developed in the last decades. In this work, the spectral finite element method (SFEM), cf. [1] and [2], is under investigation, which originates from the computational analysis in geophysics, cf. [3]. The basic ideas are illustrated in the following with emphasis on plane strain elements.

SPECTRAL FINITE ELEMENTS IN THE TIME DOMAIN

Shape functions for spectral finite elements

The shape functions for SFEM are built by the Lagrangian polynomials which read in the one-dimensional case with coordinate ξ

$$L_j^n(\xi) = \prod_{\substack{k=1 \\ k \neq j}}^{n+1} \frac{\xi - \xi_k}{\xi_j - \xi_k}. \tag{1}$$

Here, n is the degree of the polynomial with n+1 interpolation points and j is the node number with non-vanishing function value. As shown in equation (1) the position of ξ_k is user-defined. In this case the interpolation points are placed at the Gauss-Lobatto-Legendre (GLL) points which are obtained by the solution of

$$(1-\xi^2)P_n'(\xi) = 0\,. \tag{2}$$

Here, P_n' denotes the first derivative of a Legendre polynomial of degree n and the term $(1-\xi^2)$ ensures two fixed interpolation points at the boundaries of the interval [-1, 1]. The 2D shape functions result by multiplying the in ξ-, resp. η- direction individual ordered 1D Langrangian polynomials. Motivation for selecting the GLL points as interpolation points of the 2D shape functions is the employed GLL integration scheme. The interpolation points of the shape functions as well as the integration points of the GLL quadrature are located at the GLL points.

In the two-dimensional case, the element stiffness matrix **K** and the element mass matrix **M** are computed by

$$\mathbf{K} = \int_{\Omega_e} \mathbf{B}^T \mathbf{C}\mathbf{B} d\Omega = t \sum_{ij} w_i w_j \mathbf{B}(\xi_i, \eta_j) \mathbf{C}\mathbf{B}(\xi_i, \eta_j) \det \mathbf{J}(\xi_i, \eta_j), \tag{3}$$

$$\mathbf{M} = \rho_0 \int_{\Omega} \mathbf{N}^T \mathbf{N} d\Omega = \rho_0 t \sum_{ij} w_i w_j \mathbf{N}(\xi_i, \eta_j) \mathbf{N}(\xi_i, \eta_j) \det \mathbf{J}(\xi_i, \eta_j). \tag{4}$$

Here, w_i and w_j are weighting factors at the integration points, t is the element thickness and ρ_0 denotes the density. By evaluation of equation (4) the function values at the integration points are multiplied. With just one non-zero function value the GLL interpolation points demonstrate their main advantage. Compared to the fully populated mass matrix which results using conventional Gauss integration points, the GLL integration points provide a diagonalised mass matrix.

Time integration

The existence of a diagonal mass matrix in SFE analysis may be advantageous for the time integration. Regardless of the integration scheme under consideration, the equation of motion reads after discretisation of the time $\mathbf{K}_{\text{eff}}\, \mathbf{u}_{t+\Delta t} = \mathbf{F}_{\text{eff}}$.

In implicit time integration schemes, e.g. the Newmark method, the effective stiffness matrix $\mathbf{K}_{\text{eff}}$ depends on the stiffness, damping and mass matrices **K**, **D** and **M**. However, in explicit time integration schemes, the effective stiffness matrix $\mathbf{K}_{\text{eff}}$ solely depends on the mass and damping matrices:

$$\mathbf{K}_{eff}^{\exp} = \frac{\mathbf{M}}{\Delta t^2} + \frac{\mathbf{D}}{2\Delta t} \tag{5}$$

Under the assumption of Rayleigh damping one obtains $\mathbf{D} = \alpha_0\mathbf{M} + \alpha_1\mathbf{K}$. Thus, $\alpha_1 = 0$ gives a diagonal damping matrix and finally $\mathbf{K}_{\text{eff}}$ becomes diagonal. This fact enables a more efficient integration in time than using an implicit time integration scheme. However, in the analysis of wave propagation special care has to be taken in a proper choice of the time step Δt. In the following, all numerical calculations are performed without damping ($\alpha_0 = 0$).

NUMERICAL CALCULATION

Beforehand, the correctness of spectral finite elements assembled in an existing program code is validated by means of [4] to which reference is made.

Numerical Model of a 7-ply composite

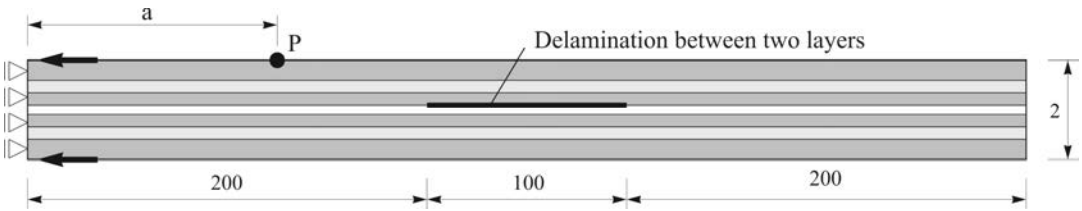

Figure 1. Model of the 7-ply laminate for the numerical simulation [mm].

In this study, the wave propagation in a quasi-isotropic 7-ply composite with dimensions shown in Figure 1 is investigated using spectral finite elements. The first (top) and seventh (bottom) laminas are 2/2 twill weaves (woven fabrics), the central layer is a plane weave and the other ones are unidirectional (UD) fibre-reinforced layers. The stacking sequence of this laminate is [0/+45/-45/0/-45/+45/0]. Material properties and thickness of each layer are listed in Table 1. These parameters are experimentally determined.

Table 1. Material properties and thickness.

	E_1 [GPa]	E_2 [GPa]	E_3 [GPa]	G_{12} [GPa]	G_{23} [GPa]	G_{31} [GPa]	ν_{12}	ν_{23}	ν_{31}	ρ [$\cdot 10^3$ kg/m³]	t [mm]
twill weave	49.6	49.6	6.1	3.56	2.67	2.67	0.030	0.322	0.034	1.52	0.4
UD - layer	127.5	7.9	-	5.58	2.93	-	0.273	-	-	1.55	0.25
plane weave	53.4	53.4	6.4	3.83	2.87	2.87	0.030	0.319	0.033	1.56	0.2

The symmetric (S_0), resp. antisymmetric (A_0), mode is excited by two same, resp. opposite, orientated single loads at the top and bottom surface of the plate (distance between axis of symmetry and excitation point: 2.5 mm). The laminate is discretised

by 100 elements in length and one element in height per layer. Each element consists of 7×3 nodes.

Phase velocity in the intact 7-ply composite

A first investigation attends to the phase velocity in the intact 7-ply laminate. Therefore, the structure is excited by a time harmonic signal with a frequency of 25 kHz. The computed wave lengths amount to $\lambda_{sym} \approx 225$ mm, resp. $\lambda_{anti} \approx 26$ mm and lead to the phase velocities at about $c_{p,sym} \approx 5500$ m/s, resp. $c_{p,anti} \approx 680$ m/s, shown in Figure 2. Herein, crosses mark the velocities calculated with spectral finite elements (SFEM), circles denote experimentally determined velocities and the solid lines sign the calculated dilatational (Fig. 2 a) and flexural (Fig. 2 b) wave velocity using the classical laminate theory (CLT), cf. [5].

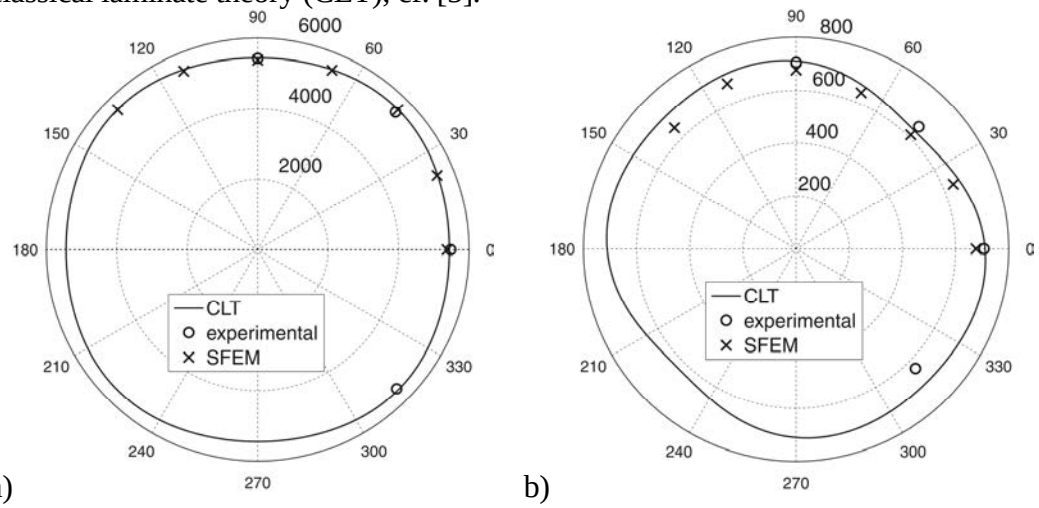

a) b)

Figure 2. Phase velocity of the a) symmetric and b) antisymmetric Lamb wave mode at different propagation angles.

The typical circular wave propagation of the S_0-mode in quasi-isotropic materials is in evidence in Figure 2 a). The phase velocity computed using SFE shows a very good agreement with the experimentally determined velocity as well as the calculated velocity when using the CLT for all investigated propagation angles. A maximum deviation of 2 per cent between numerical (SFEM) and experimental results is obtained.

In Figure 2 b) SFEM- and CLT- results coincide moderately well with the experimentally determined velocities. Here, the maximum deviation amounts to acceptable 7 per cent. The diagonally distorted propagation shape is a consequence of the varying moments of inertia of the single UD- layers (+45°/-45°).

Wave propagation in 7-ply composite with delamination

A delamination of 100 mm is implemented between two layers for the analysis of wave propagation in a damaged composite (see Fig. 1). The delamination is realised by unjoined nodes at both involved layer surfaces seen in Figure 3. The gap just demonstrates the node-element connection and is non-existent in the numerical model. A transient Hanning windowed five cycle sine burst at a frequency of 200 kHz is initiated. The wave lengths of the S_0- and A_0-waves ($\lambda_{sym} \approx 28$ mm and $\lambda_{anti} \approx 6$ mm)

are considerably shorter than the delamination and let expect a good interaction with it. The displacements are observed at point P (a = 125 mm), see Figure 1.

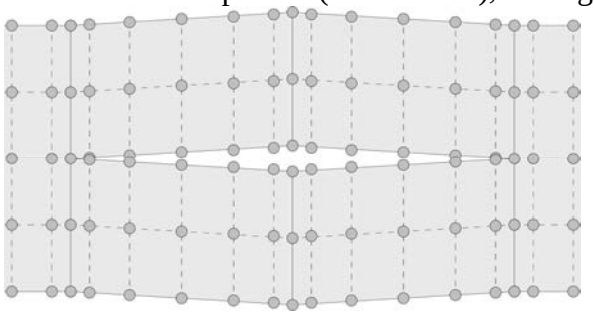

Figure 3. Delamination realised by node separation.

The displacements in the primary oscillation direction of each mode are plotted in Figure 4 and 5, being in-plane (u_x) for S_0 and out-of-plane (u_y) for A_0. The upper graph in both figures shows the temporal plot of an intact plate, the second and third curve presents the temporal plot of the plate with a delamination between layer 1 and 2, resp. 3 and 4.

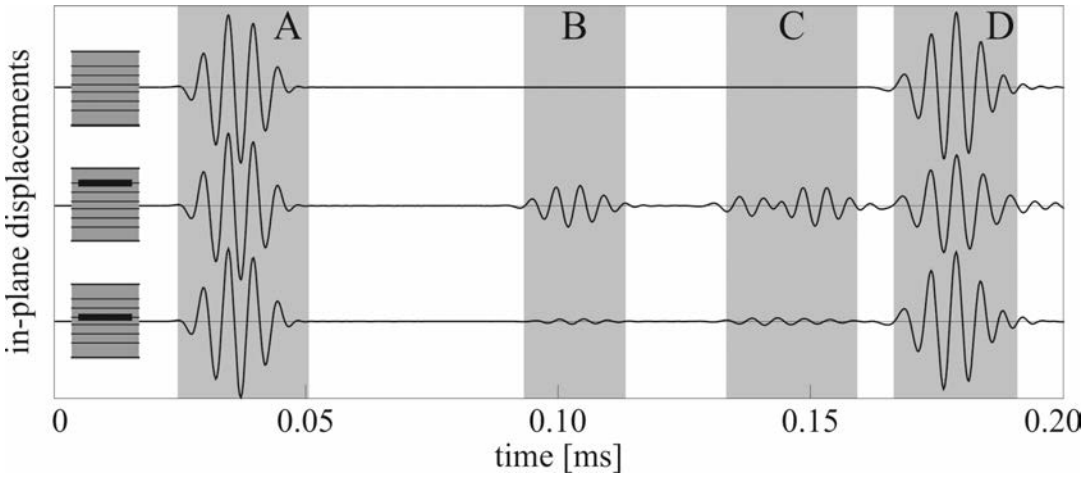

Figure 4. In-plane displacements u_x of S_0-mode plotted over time at point P.

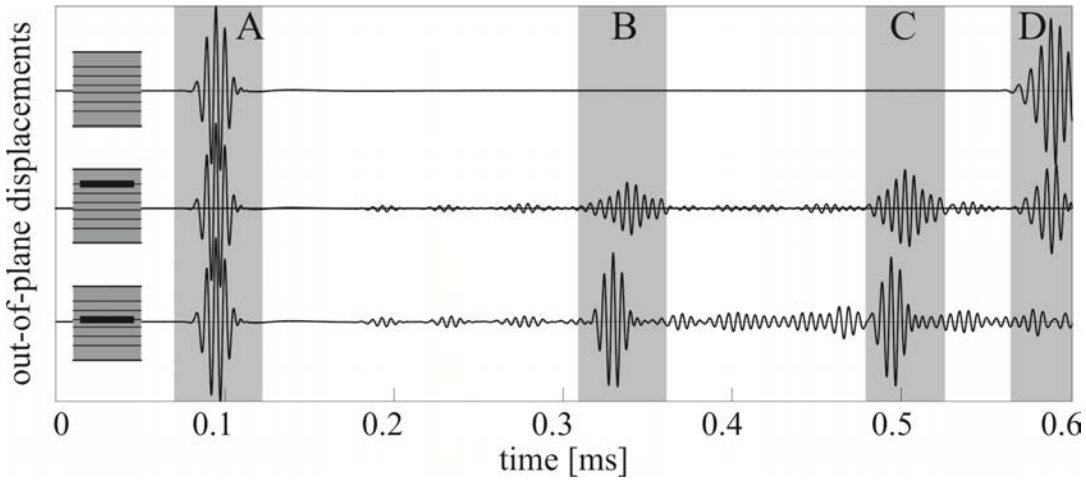

Figure 5. Out-of-plane displacements u_y of A_0-mode plotted over time at point P.

The incident wave (area A) passes the beginning of the delamination without mentionable reflections. Significant oscillations occur when the wave packet is travelling across the end of the delamination, as also noted in reference [6]. These reflections are visible in area B. The amplitudes in area C show these reflections after another reflection at the left end of the plate. Area D illustrates the main wave group reflected at the right edge of the composite plate.

The bottom S_0 displacement curve in Figure 4 shows very small amplitudes in areas B and C compared to the middle displacement curve with delamination between first and second layer. This is due to the nearly centrally arranged position of the delamination in height (between third and fourth layer), since shear forces of the S_0-mode becomes zero in the mid-plane of a symmetric geometrical set-up. Therefore, the position-independent A_0-waves (see oscillations in areas B and C of bottom displacement curve in Figure 5) are more suitable for the detection of delaminations.

Modelling of delamination using node separation or contact elements (ANSYS)

In this section, the prior calculated displacement curves of a delaminated composite originated by separated nodes in the damaged region are compared with numerical computations using conventional finite elements (FE) with integrated contact elements.

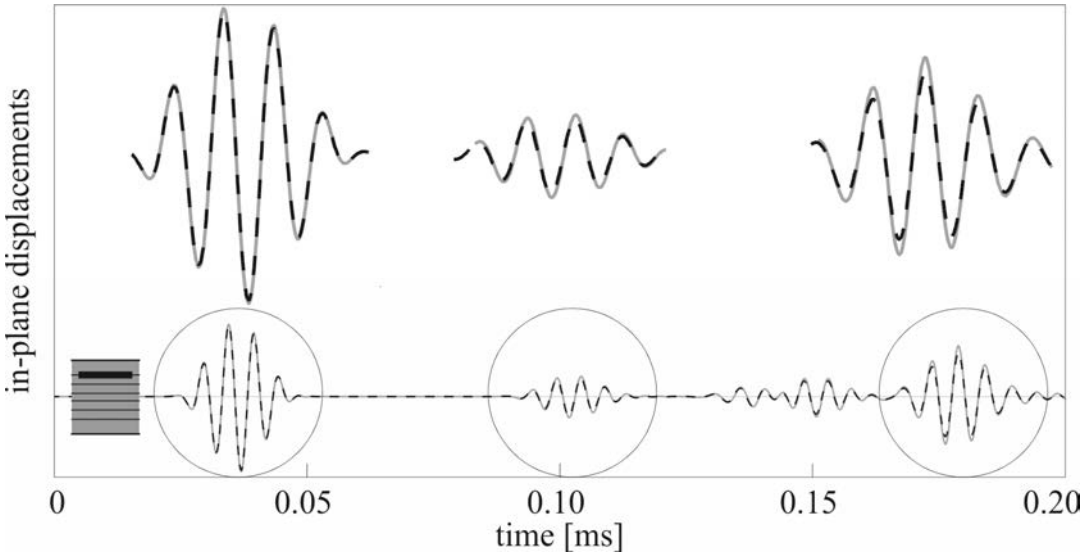

Figure 6. Comparison of in-plane displacements u_x of S_0-mode calculated with SFE (solid grey line) and conventional FE (dashed black line). Both numerical models include delaminations by node separation.

First of all to gain a realistic assessment, the SFE-model (with 700 elements and 7x3 nodes per element) and the FE-model (14000 elements and 8 nodes per element) are contrasted. The enlarged plots in Figure 6 show a qualitatively good agreement of both models (SFE - solid grey line and FE - dashed black line) which is underlined by a normalised amplitude error (amounts to 10 per cent) and a more significant normalised phase error (less than 1 per cent). In this case, the normalised amplitude error is the root mean square error (RMSE) of both temporal plots referred to the effective value of the FE-computation and the phase error is the arithmetic mean scaled by the expected cycle duration (T = 1/frequency = $5 \cdot 10^{-5}$ sec).

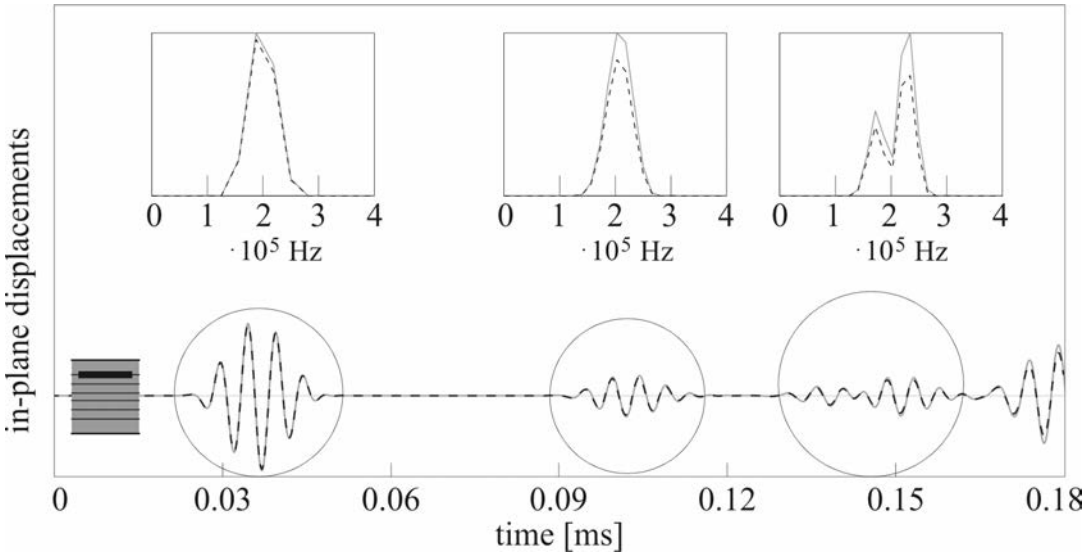

Figure 7. Amplitude spectrum (upper plots) of different S_0-wave packets (solid grey line - SFE-model; dashed black line - FE-model).

Figure 7 shows the in-plane displacement curves of the symmetric wave in the "node-separated" SFE-model (solid grey line) and the FE-model with contact elements (dashed black line) including the amplitude spectrum of individual wave packets. The distinct maxima at approximately 200 kHz in the left and middle plots of the amplitude spectrum coincide well for both models. Also the main (230 kHz) and side lobe (170 kHz) in the right plot are equally marked. In the case of S_0-wave propagation the delamination edges do not seem to interact with each other which allows a very good approximation by the use of a simplified delamination model made up of separated nodes.

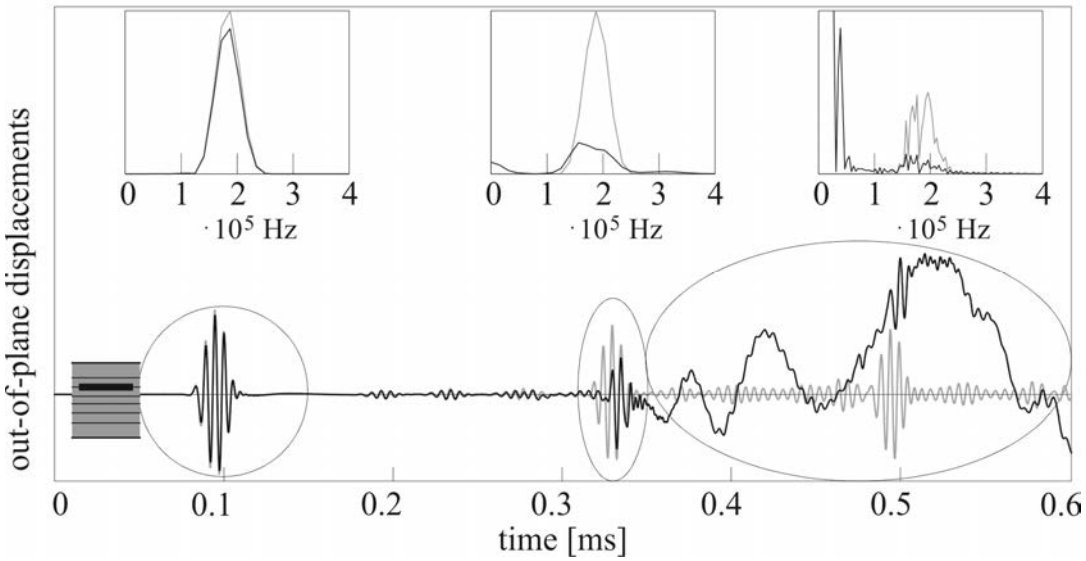

Figure 8. Amplitude spectrum (upper plots) of different A_0-wave packets (grey line - SFE-model; black line - FE-model).

As shown in Figure 8 the A_0- mode is also analysed concerning its temporal plot (here out-of-plane displacements) and its frequency spectrum of individual time ranges in the contact-model (FE-model: black line) and the "node-separated"-model (SFE-model: grey line). In both delamination models the incident wave (encircled

wave packet left hand side) and first minimal reflections of the left end of the delamination (time interval: 0.18 ms - 0.25 ms) agree very well. However, obviously differences are beginning to occur after 0.3 ms. Since the center plot of amplitude spectrum of the contact-model (black line) just indicates extremely low frequencies the right one shows a significant marked main lobe in the low frequency range. This implies that the boundaries of the delamination start to interact with each other after the travelling wave passed the right end of the delamination.

CONCLUSION

In this paper, the method of spectral finite elements is presented and utilised for the computation of wave propagation in an anisotropic 7-layered composite. A high conformity between numerically computed, experimentally determined and by the classical laminate theory calculated phase velocities at different propagation angles is shown using the example of an undamaged composite.

Furthermore, the wave propagation in the same composite with an artificial delamination implemented by separated nodes is investigated. This study shows an ideal suitability of A_0-waves for the detection of variously (in height) positioned delaminations, where reflections from the far delamination end appear anyway.

Finally, the employed delamination model obtained by node separation is compared with a delamination model made up of contact elements. For the observation of S_0-wave propagation the simplified model exposed to be a very good approximation, whereas A_0-wave propagation cannot sufficiently be described by the delamination model with separated nodes.

REFERENCES

1. Hennings, B. and R. Lammering. “Modelling of wave propagation in layered plane strain structures using spectral finite elements,” In: *Mechanical Response of Composites*, Hannover, Germany, September 2011, p. 411-418.
2. Kudela, P., et al. 2007. “Modelling of wave propagation in composite plates using the time domain spectral element method,” *J. Sound Vib.*, 302: 728–745.
3. Komatitsch, D. and J. Tromp. 1999. “Introduction to the spectral element method for three-dimensional seismic wave propagation,” *Geophys. J. Int.*, 139: 806–822.
4. Peng, H., et al. 2010. “Concise analysis of wave propagation using the spectral element method and identification of delamination in CF/EP composite beams,” *Smart Mater. Struct.*, 19: 1–11.
5. Altenbach, H., et al. 1996. *Einführung in die Mechanik der Laminat- und Sandwichtragwerke*. Deutscher Verlag für Grundstoffindustrie, Stuttgart.
6. Hayashi, T. and K. Kawashima. 2002. “Multiple reflections of Lamb waves at a delamination,” *Ultrasonics*, 40: 193-197.